Effect of carrier confinement on exchange coupling in dilute magnetic semiconductors with self-organized nanocolumns

S. Caprara,[1,2] V. N. Men'shov,[1,3] V. V. Tugushev,[1,3] P. M. Echenique,[1,4] and E. V. Chulkov[1,4]
[1]*Donostia International Physics Center (DIPC), P. de Manuel Lardizabal 4, 20018 San Sebastián, Basque Country, Spain*
[2]*CRS SMC, CNR-INFM and Dipartimento di Fisica, Università di Roma "Sapienza", Piazzale Aldo Moro 2, 00185 Roma, Italy*
[3]*RRC Kurchatov Institute, Kurchatov Square 1, 123182 Moscow, Russia*
[4]*Departamento de Física de Materiales, Facultad de Ciencias Químicas, UPV/EHU, Apdo. 1072, 20080 San Sebastián, Basque Country, Spain and Centro Mixto, CSIC-UPV/EHU, Apdo. 1072, 20080 San Sebastián, Basque Country, Spain*
(Received 16 September 2008; published 9 January 2009)

The "carrier-confinement" model for phase-separated dilute magnetic semiconductors is proposed, in which the carrier scattering by ferromagnetic strings embedded into a semiconductor host leads to the appearance of quasi-one-dimensional spin-polarized states inside the energy gap of the three-dimensional spectrum. Quasiparticle excitations from these states to the band edge mediate an efficient interstring exchange even in the absence of free carriers in the host. The related exchange integral can switch between ferromagnetic and antiferromagnetic with varying both the interstring distance and the filling of the quasi-one-dimensional spin-polarized states. We discuss the applicability of our model for the description of the magnetic behavior of the array of Mn-rich nanocolumns inserted into a Mn-depleted host in phase-separated (Ge,Si):Mn alloys.

DOI: 10.1103/PhysRevB.79.035202 PACS number(s): 73.40.Sx

I. INTRODUCTION

There exist compelling evidence for magnetic order in group-IV semiconductors (SC=Ge,Si) dilute alloys with 3*d*-transition metals, but its origin is still controversial. Multiple studies reveal that magnetism may not be the intrinsic property of these dilute magnetic semiconductors (DMSs), but rather arises from magnetic peculiarities of clusters enriched in transition metals (contaminants, containing germanides or silicides of the transition metal) in the SC matrix, which appear due to the phase separation.

For Ge-based DMS, ferromagnetic (FM) order up to 110 K has been reported in $Ge_{1-x}Mn_x$ grown by molecular-beam epitaxy (MBE) at $x=0.033$ and attributed to Mn_nGe_m FM nanoclusters (of typical size of 2–6 nm) with higher Mn concentration (10–15 %) than in the surrounding matrix, rather than to isolated Mn impurities in the Ge host.[1] The FM transition at $T_c=285$ K and the antiferromagnetic (AFM) transition at $T_n=150$ K were reported in highly Mn-doped (up to 6%) Ge single crystals obtained by solid solutions.[2] On the other hand, to interpret the results on the magnetic coupling in Ge:Mn, Li *et al.*[3] proposed to introduce two different temperatures for FM ordering, T_c^* and T_c. The higher critical temperature T_c^* marks the onset of local ferromagnetism, whereas the global ferromagnetism takes place only at a much lower transition temperature T_c. The values of T_c found for a sample with 5 at. % Mn are on the order of 10 K (while the values of T_c^* are on the order of 300 K), which indicates that $Ge_{1-x}Mn_x$ is far from being a high-T_c DMS. Moreover, according to Ref. 3, transport measurements revealed the insulating behavior of $Ge_{1-x}Mn_x$ over the entire temperature range considered, so that the Fermi level is located below the mobility edge of the Mn-induced impurity band. Gareev *et al.*[4] reported that indirect FM exchange in Ge:(Mn,Fe) insulating-type DMS is mediated by localized holes with concentration $n=10^{20}$ cm^{-3} and mobility $\mu=10$ cm^2/(V s). The authors of Ref. 5 provided insights into the correlation of the magnetic and structural properties of $Ge_{0.95}Mn_{0.05}$ films fabricated with low-temperature MBE. The individual Mn_5Ge_3 nanoprecipitates turn FM and carry large magnetic moments, which react freely to an external applied field, like a superparamagnet. Recent photoelectron emission, x-ray-absorption spectroscopy, and magnetization measurements on $Ge_{0.96}Mn_{0.04}$ single crystalline films have shown the coexistence of substitutional Mn atoms and Mn_5Ge_3 or $Mn_{11}Ge_8$ nanoprecipitates, dispersed in the Ge host.[6,7]

For Si-based DMS, the above room-temperature ferromagnetism has been achieved in Mn ion implanted Si with Mn concentrations of 0.1–0.8 at. %.[8] The x-ray-absorption studies indicate that Mn ions in these systems are located neither in the substitutional nor in the interstitial position of the Si lattice and form clusters with five to eight nearest-neighbor atoms.[9] On the other hand, there were no indications for Mn substituting Si, either in the as-implanted or in the rapidly annealed samples, and the observed ferromagnetism with a saturation moment of $0.21\mu_B$ per implanted Mn ion was attributed to $MnSi_{1.7}$ nanoparticles (of typical size of 5–20 nm).[10] The Curie-Weiss law for the magnetic susceptibility was observed in Mn-doped amorphous a-$Si_{1-x}Mn_x$ ($0.005<x<0.175$) films, but with extremely small total moment; the measurements suggest that only a small part of Mn ions contributes to the magnetization and the moments are quenched for the majority of Mn ions.[11]

Strictly speaking, it may be difficult to unambiguously distinguish strongly inhomogeneous DMS containing intermetallic compounds or Mn-rich clusters from a proper spatially uniform material in $(Ge,Si)_{1-x}Mn_x$ alloys with Mn contents of a few percent. However, it was recently established by independent groups of investigators that, in low-temperature MBE as-grown $(Ge,Si)_{1-x}Mn_x$ alloys, the dopant exhibits a remarkable tendency toward self-organization into arrays of Mn-rich clusters ("nanocolumns" or "nanopipes") in the Mn-depleted matrix.[12–15] In Ref. 12, the

$Si_{1-x}Mn_x$ films with $0.005<x<0.035$ grown on a Si(100) substrate were investigated using reflection high-energy electron diffraction. It was demonstrated that at small Mn content and low growing temperature, Mn-rich nanometer-sized nodules form near the bottom of the film and seed the formation of vertical nanopipes extended to the surface. Unfortunately, no detailed information on the average diameter of the nanopipes and internanopipe distance was communicated. In Refs. 13 and 14 structural and magnetic properties of $Ge_{1-x}Mn_x$ films with $0.01<x<0.11$ grown on a Ge(001) substrate were investigated by transmission electron microscopy, electron energy-loss spectroscopy, and x-ray diffraction. The formation of Mn-rich nanocolumns embedded into a nearly pure Ge matrix was reported. The nanocolumns have a fairly uniform size distribution with an average column diameter of 3 nm and a pair-correlation length of 10 nm; FM ordering at $T>400$ K and giant positive magnetoresistance (MR) were observed in this system.

On the other hand, magnetic and transport features in the phase segregated $Ge_{1-x}Mn_x$ alloys are extremely sensitive to the precise location and distribution of the magnetic dopant.[15] In the as-grown material, FM columns are embedded into a crystalline Ge matrix in which substitution acceptors and interstitial donors are almost perfectly compensated. These insulating materials exhibit AFM interaction between adjacent columns and giant positive MR. The dopant atoms are redistributed upon postannealing, resulting into an increase in the concentration of uncompensated acceptors, which provides a FM coupling between adjacent columns and global ferromagnetism with small negative MR.

In this work, we discuss a mechanism for the formation of the magnetic order within a self-organized nanocolumn and for the global magnetic ordering in the phase-separated dilute (Ge,Si):Mn alloys with a columnar topology, accounting for the results of Refs. 12–15. We first consider a model which takes into account the main ingredients to describe the physics of an isolated nanocolumn embedded into a semiconducting host, approximated as an ideal FM string. These are the charge redistribution in the matrix around the nanocolumn, the hybridization between the host and the dopant electron states, and the intra-atomic Coulomb interactions of two electrons within a dopant ion, which is the driving force of magnetism. We then derive an approximate Hamiltonian which describes the coupling of the host electron states to a FM string, and consider a model of two parallel FM strings embedded into the insulating matrix, to clarify the mechanism of exchange coupling between strings and describe its dependence on the interstring distance and on the Fermi-level position.

II. MODEL FOR A FM STRING IN A SEMICONDUCTING MATRIX

To describe the occurrence of ferromagnetism within an isolated nanocolumn, we introduce a model which treats the nanocolumn as an ideal one-dimensional string of dopant ions and accounts for the relevant degrees of freedom, while neglecting orbital degrees of freedom, which are responsible for the higher value of the FM spin, resulting from Hund's rule within the d orbitals, but do not play an important role in the formation of a ferromagnetic state. The position vector within our system is $\mathbf{R}=(\mathbf{r},z)$, with z parallel to the string, which is located at $\mathbf{r}=0$. The corresponding wave vector is $\mathbf{K}=(\mathbf{k},\kappa)$.

Having in mind to discuss here the general mechanism for the onset of magnetism, rather than the quantitative details, for simplicity, we consider the situation in which the SC valence band is deep, and will be ignored, whereas the conduction band, arising from a single s orbital, can be reasonably described, within an effective-mass approximation, by the Hamiltonian

$$\mathcal{H}_s=\sum_{\mathbf{k}}\sum_{\kappa}\sum_{\sigma}\varepsilon(\mathbf{K})s^{+}_{\mathbf{k},\kappa;\sigma}s_{\mathbf{k},\kappa;\sigma}, \tag{1}$$

where $s^{(+)}_{\mathbf{k},\kappa;\sigma}$ annihilates (creates) an electron with wave vector $\mathbf{K}=(\mathbf{k},\kappa)$ and spin projection $\sigma=\uparrow,\downarrow$, and the conduction-band spectrum is

$$\varepsilon(\mathbf{K})=\frac{\mathbf{k}^2}{2m^*_{\perp}}+\frac{\kappa^2}{2m^*_{\parallel}}\equiv\varepsilon_{\perp}(\mathbf{k})+\varepsilon_{\parallel}(\kappa). \tag{2}$$

The Hamiltonian of an ideally isolated string is

$$\mathcal{H}_d=\sum_{\kappa}\sum_{\sigma}\varepsilon_d d^{+}_{\kappa;\sigma}d_{\kappa;\sigma}+I\sum_{i}n_{d,\uparrow}(z_i)n_{d,\downarrow}(z_i), \tag{3}$$

where $d^{(+)}_{\kappa;\sigma}$ annihilates (creates) an electron with wave vector κ and spin σ on a d orbital of the string. For simplicity, we assume a single orbital. We also neglect the small overlap of d orbitals at different sites along the string, taking a dispersionless level ε_d. This assumption does not play a relevant role since d electrons become mobile mainly due to the hybridization with the SC s orbitals. The interaction between two electrons in the same d orbital, which is the driving force of magnetism, is described by the Hubbard term of strength I. We assume that the electrons are localized at the sites z_i (with $\mathbf{r}_i=0$), and $n_{d,\sigma}(z_i)$ represents the number of d electrons with spin σ on a given site along the string.

When the string is inserted into the SC matrix, various effects arise. Those which are relevant to the formation of a spin-polarized state are the hybridization between the electron state of the dopant and of the SC host (in our model, s-d hybridization), $\tilde{V}(\mathbf{r},z-z')$, and the modulation of the local chemical potential $\tilde{U}(\mathbf{r})$, ruling the charge redistribution within the SC matrix around the string. Both effects preserve the translational invariance *along* the string. The simplest approximation consists of describing these effects as contact terms at $\mathbf{r}=0$ and $z=z'$, corresponding to the Hamiltonians

$$\mathcal{H}_{s\text{-}d}=\frac{1}{\sqrt{N_{\perp}}}\sum_{\mathbf{k}}\sum_{\kappa}\sum_{\sigma}(\tilde{V}d^{+}_{\kappa;\sigma}s_{\mathbf{k},\kappa;\sigma}+\text{H.c.}), \tag{4}$$

$$\mathcal{H}_{\text{loc}}=\frac{\tilde{U}}{N_{\perp}}\sum_{\mathbf{k},\mathbf{k}'}\sum_{\kappa}\sum_{\sigma}s^{+}_{\mathbf{k},\kappa;\sigma}s_{\mathbf{k}',\kappa;\sigma}, \tag{5}$$

where $N_{\perp}$ is the number of $\mathbf{k}$ values allowed within the first Brillouin zone by the boundary conditions. The first term describes a set of independent two-dimensional Anderson models, labeled by the dummy index κ.

We treat the Hubbard term in the Hartree approximation, and factorize the interaction as $n_{d,\uparrow}(z_i)n_{d,\downarrow}(z_i) \to n_{d,\uparrow}n_{d,\downarrow}(z_i) + n_{d,\downarrow}n_{d,\uparrow}(z_i) - n_{d,\uparrow}n_{d,\downarrow}$, where $n_{d,\sigma}=\langle n_{d,\sigma}(z_i)\rangle$ is the average number of electrons with spin σ in a d orbital. This yields two spin-dependent Hartree d levels $\varepsilon_{d,\sigma}=\varepsilon_d+In_{d,-\sigma}$.

The quantum-mechanical problem associated with the Hamiltonian $\mathcal{H}_s+\mathcal{H}_d+\mathcal{H}_{s\text{-}d}+\mathcal{H}_{\rm loc}$, with the Hubbard term linearized after the Hartree factorization, can be dealt with by standard techniques, which yield the Green's functions

$$G_{dd}=\frac{\tilde{U}(1-\tilde{D})G^0_{dd}}{\tilde{U}(1-\tilde{D})-|\tilde{V}|^2\tilde{D}G^0_{dd}}, \tag{6}$$

$$G_{ss}(\mathbf{k},\mathbf{k}')=G^0_{ss}(\mathbf{k})\delta_{\mathbf{k},\mathbf{k}'}+\frac{\tilde{U}}{N_\perp}G^0_{ss}(\mathbf{k})G^0_{ss}(\mathbf{k}') \times\frac{\tilde{U}+|\tilde{V}|^2G^0_{dd}}{\tilde{U}(1-\tilde{D})-|\tilde{V}|^2\tilde{D}G^0_{dd}}, \tag{7}$$

where an implicit diagonal dependence on κ, on the (complex) frequency ω, and on the spin index σ is understood. Here, $G^0_{dd}=(\omega-\varepsilon_d)^{-1}$ is the Green's function of an ideally isolated string, $G^0_{ss}(\mathbf{K})=[\omega-\varepsilon_\perp(\mathbf{k})-\varepsilon_\parallel(\kappa)]^{-1}$ is the Green's function of the electrons in the bulk SC, and

$$\tilde{D}\equiv\frac{\tilde{U}}{N_\perp}\sum_{\mathbf{k}}G^0_{ss}(\mathbf{K})=\tilde{u}\ln\left[1+\frac{\Lambda}{\varepsilon_\parallel(\kappa)-\omega}\right]. \tag{8}$$

We introduced the dimensionless parameter $\tilde{u}\equiv -a^2m^*_\perp\tilde{U}/(2\pi\hbar^2)$, a is a lattice spacing, and $\Lambda\sim\hbar^2/(2m^*_\perp a^2)$ is a bandwidth cutoff for the two-dimensional band $\varepsilon_\perp(\mathbf{k})$. The equation $\tilde{D}=1$ describes one-dimensional bound states (for $\tilde{U}<0$, i.e., $\tilde{u}>0$) or antibound states (for $\tilde{U}>0$, i.e., $\tilde{u}<0$) formed near the edge of the SC bulk conduction band due to the charge redistribution around the string. These states are localized in the directions perpendicular to the string, but propagating along the string. In this paper, we treat the case $\tilde{u}>0$, when bound states at energies $\bar{\varepsilon}(\kappa)=\varepsilon_\parallel(\kappa)-\Lambda(e^{1/\tilde{u}}-1)^{-1}$ are split off the bottom of the SC conduction band. At weak coupling, $\tilde{u}\ll 1$ and $\bar{\varepsilon}(\kappa)\approx\varepsilon_\parallel(\kappa)-\Lambda e^{-1/\tilde{u}}$; at strong coupling, $\tilde{u}\gg 1$ and $\bar{\varepsilon}(\kappa)\approx\varepsilon(\kappa)-\Lambda\tilde{u}$. In the following, we do not need the expressions of the G_{sd} and G_{ds} Green's functions.

The s-d hybridization removes the poles of the Green's function G_{ss} at $\bar{\varepsilon}(\kappa)$ and promotes instead one-dimensional s-d bands, which appear as poles of G_{dd} and $G_{ss}(\mathbf{k},\mathbf{k}')$. Unfortunately, we could not obtain simple analytical expressions for the momentum-integrated Green's functions

$$\bar{G}_{dd}(\omega)=\frac{1}{N_\parallel}\sum_\kappa G_{dd}, \tag{9}$$

$$\bar{G}_{ss}(\omega)=\frac{1}{N_\parallel}\sum_{\mathbf{k},\kappa}G_{ss}(\mathbf{k},\mathbf{k}), \tag{10}$$

where $N_\parallel$ is the number of κ values allowed within the first Brillouin zone by the boundary conditions. The sums over κ were then performed numerically over a closely spaced mesh.

The densities of states are then found as $\mathcal{N}_\ell(\omega)=-\frac{1}{\pi}\mathrm{Im}\,\bar{G}_{\ell\ell}(\omega+i\delta)$, with $\ell=s,d$ and $\delta=0^+$. In our numerical analysis we take $\delta/W=10^{-3}$, where W is the bandwidth cutoff. This value is at least 2 orders of magnitude smaller than the other dimensionless energy scales.

For numerical simplicity, we work at fixed chemical potential μ and zero temperature. When the system is spin polarized, the number of electrons with spins $\uparrow$ and $\downarrow$ is different and the source of this unbalance is self-consistently related to the splitting of the d level, $\varepsilon_{d,\sigma}=\varepsilon_d+In_{d,-\sigma}$. Let us indicate with $\mathcal{N}^\sigma_\ell(\omega)$ the density of states (DOS) for spin σ, which depends self-consistently on $n_{d,-\sigma}$. Then, the two coupled self-consistency equations which determine $n_{d,\sigma}$ have the form

$$n_{d,\sigma}=\int_{-\infty}^{\mu}d\omega\mathcal{N}^\sigma_d(\omega), \tag{11}$$

with $\sigma=\uparrow,\downarrow$. By expressing, e.g., $n_{d,\downarrow}$ as a function of $n_{d,\uparrow}$ and then substituting into the equation for $n_{d,\uparrow}$, the two equations are decoupled, and a single equation of the form $n_{d,\uparrow}=F(n_{d,\uparrow})$ is obtained, which can be efficiently solved, e.g., by iterative bisection. The procedure is lengthy since $\mathcal{N}^\sigma_d(\omega)$ has to be numerically evaluated at each step due to the lack of a simple analytical expression.

Once the self-consistent value of $n_{d,\uparrow}$ is found, one can proceed with the straightforward evaluation of $n_{d,\downarrow}$ and

$$n_{s,\sigma}=\int_{-\infty}^{\mu}d\omega\mathcal{N}^\sigma_s(\omega). \tag{12}$$

Similarly, the thermodynamic grand-canonical potential can be calculated as

$$\Omega=\sum_{\ell=s,d}\sum_{\sigma=\uparrow,\downarrow}\int_{-\infty}^{\mu}d\omega(\omega-\mu)\mathcal{N}^\sigma_\ell(\omega)-In_{d,\downarrow}n_{d,\uparrow}, \tag{13}$$

where the last term is subtracted to avoid double counting of the Hartree energy.

For the sake of definiteness, we adopted the set of parameters $\varepsilon_d/W=-0.5$, $\tilde{u}=1.0$, $|\tilde{V}|^2/(|\tilde{U}|W)=0.25$, and $\Lambda/W=2/3$, and we studied the properties of our model for varying μ/W and I/W. The zero energy level is fixed at the bottom of the three-dimensional (3D) SC conduction band $\varepsilon(\mathbf{K})\geq 0$. Since there are no free particles in the system to fill the 3D SC conduction band, only the case $\mu\leq 0$ is relevant.

We define the partial magnetizations $m_d=n_{d,\uparrow}-n_{d,\downarrow}$ and $m_s=n_{s,\uparrow}-n_{s,\downarrow}$, and the total magnetization $m_{\rm tot}=m_d+m_s$. In Fig. 1 we show the phase diagram. At small I/W the system is paramagnetic (PM), but with increasing I/W the system eventually enters the spin-polarized phase. For the chosen set of parameters, at small $|\mu|/W$, this spin-polarized phase is *ferrimagnetic* (fm) with s spins antiparallel to d spins (i.e., $m_dm_s<0$). With increasing $|\mu|/W$, the number of minority s spins is reduced and the system is gradually turned into a ferromagnet (with $m_dm_s>0$). The line $m_s=0$, which separates the ferrimagnet and the ferromagnet, is shown as a dotted line in Fig. 1. For even larger $|\mu|/W$ the system be-

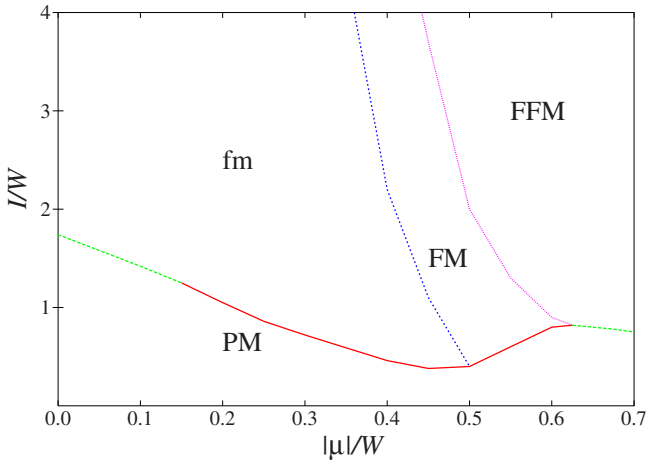

FIG. 1. (Color online) Phase diagram of the Anderson-type model for a d-metal string embedded into a bulk SC. The parameters are taken as $\varepsilon_d/W=-0.5$, $\tilde{u}=1.0$, $|\tilde{V}|^2/(|\tilde{U}|W)=0.25$, and $\Lambda/W=2/3$. The label PM indicates the paramagnetic phase, which can be metallic or insulating depending on the value of the chemical potential; the label fm indicates the ferrimagnetic phase, which is half metallic; and the label FM indicates the ferromagnetic phase, which is half metallic. The label FFM indicates a saturated ferromagnetic phase, which is insulating. The continuous line separating the PM phase from the various spin-polarized phases marks a second-order transition, whereas the dashed line corresponds to a first-order transition. The lines separating the fm and FM phases and the FM and FFM phases mark continuous changes without symmetry breaking.

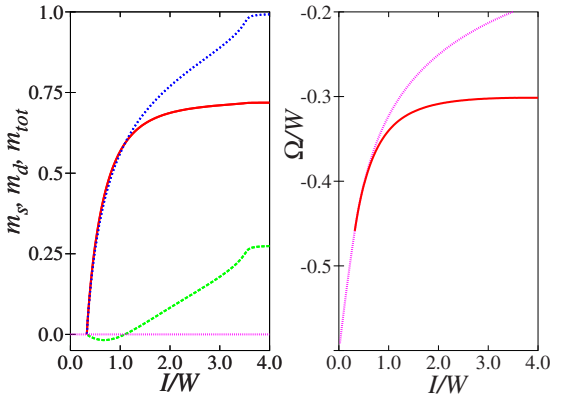

FIG. 2. (Color online) Magnetization curves (left panel: dashed line for m_s, solid line for m_d, and dotted line for $m_{\rm tot}$; the shaded line marking the zero value characterizes the PM phase) and grand-canonical thermodynamic potential (right panel: solid line for the spin-polarized phases, and shaded line for the PM phase) for the same parameters as in Fig. 1 and $\mu/W=-0.45$. For this value of the chemical potential, and the chosen set of parameters, all the possible regimes of the model are found, as it can be seen from Fig. 1. The system is PM (with $m_s=m_d=m_{\rm tot}=0$) for $I/W\leq 0.38$, fm (with $m_s m_d<0$) for $0.38<I/W<1.1$, FM (with $m_s m_d>0$) for $1.1<I/W<3.7$, and FFM (with $m_t=1$) for $I/W\geq 3.7$. The second-order PM-fm transition, at which m_d, m_s, and m_t simultaneously vanish, and the thermodynamic potential of the spin-polarized phase (solid line in the right panel) merges with the thermodynamic potential of the PM phase (shaded line in the right panel).

comes fully polarized, with the lower majority-spin band full and the lower minority-spin band empty. The line marking the onset of the fully polarized state is drawn as a thin line in Fig. 1.

In Fig. 2 we show the magnetization and thermodynamic potential at $\mu/W=-0.45$, when the system exhibits all the possible behaviors, for the chosen set of parameters. The dashed line represents the partial magnetization m_s, which is opposite to m_d (solid line) close to the PM-fm transition, vanishes at the fm-FM transition, and saturates, together with m_d, at where the fully polarized ferromagnetic (FFM) state is formed. The full magnetization is represented by the dotted line. The thermodynamic potential of the spin-polarized phase continuously joins the thermodynamic potential of the PM phase, since for the chosen value of the chemical potential the transition is of second order.

In Fig. 3 we show the DOS. The paramagnetic phase is found as metallic or insulating, depending on whether the Fermi energy crosses the upper or lower band, or is located in the gap between the two. The ferrimagnetic and ferromagnetic phases are half metallic, with the Fermi energy located within the minority-spin lower band, whereas the majority-spin lower band is full. The fully polarized ferromagnetic phase is insulating, with the Fermi energy located within the gap between the minority-spin lower band (empty) and the majority-spin lower band (full).

So far, we have investigated the mechanism for the onset of a FM state within an isolated string embedded into a SC host. To proceed further in the analysis of the mechanism for exchange coupling between two strings, we need to adopt some simplifying assumptions. In general, from the point of view of the electron states in the host, the coupling between the SC host and an isolated string is described by a frequency-dependent self-energy $\Sigma_{ss}(\omega)=\tilde{U}+|\tilde{V}|^2 G^0_{dd}(\omega)$, which can be read off Eq. (7). Within a rotationally invariant formulation, referred to a local spin-quantization axis, the self-energy can always be separated into a potential and an exchange part, $\Sigma_{ss}(\omega)=\Sigma^0_{ss}(\omega)\sigma_0+\boldsymbol{\Sigma}_{ss}(\boldsymbol{\omega})\cdot\boldsymbol{\sigma}$, where σ_0 is the unity matrix and $\boldsymbol{\sigma}$ is the vector of Pauli matrices.

The dynamical part of the self-energy describes the effect of charge and spin fluctuations within the string. In the following, we neglect the effect of these fluctuations and assume that a static approximation is sufficient to qualitatively estimate the energy of coupling between the string and the host. This amounts to treat the string as a classical object. When the self-energy $\Sigma_{ss}(\omega)$ is calculated at $\omega=0$, the Green's function G_{ss} becomes the Green's function of a Bloch electron in an external field $\mathcal{V}$, which describes the effect of the string. Together with the self-energy, the external field has a potential and an exchange part, $\mathcal{V}=-(U\sigma_0+J\mathbf{M}\cdot\boldsymbol{\sigma})$, where matrix elements of effective interaction between the string and the host (U and J) are merely treated as phenomenological parameters, and $\mathbf{M}$ is the magnetic moment of the string.

III. EXCHANGE COUPLING BETWEEN TWO FM STRINGS

Let us now introduce an effective model to describe the system of two parallel FM strings embedded into a crystal-

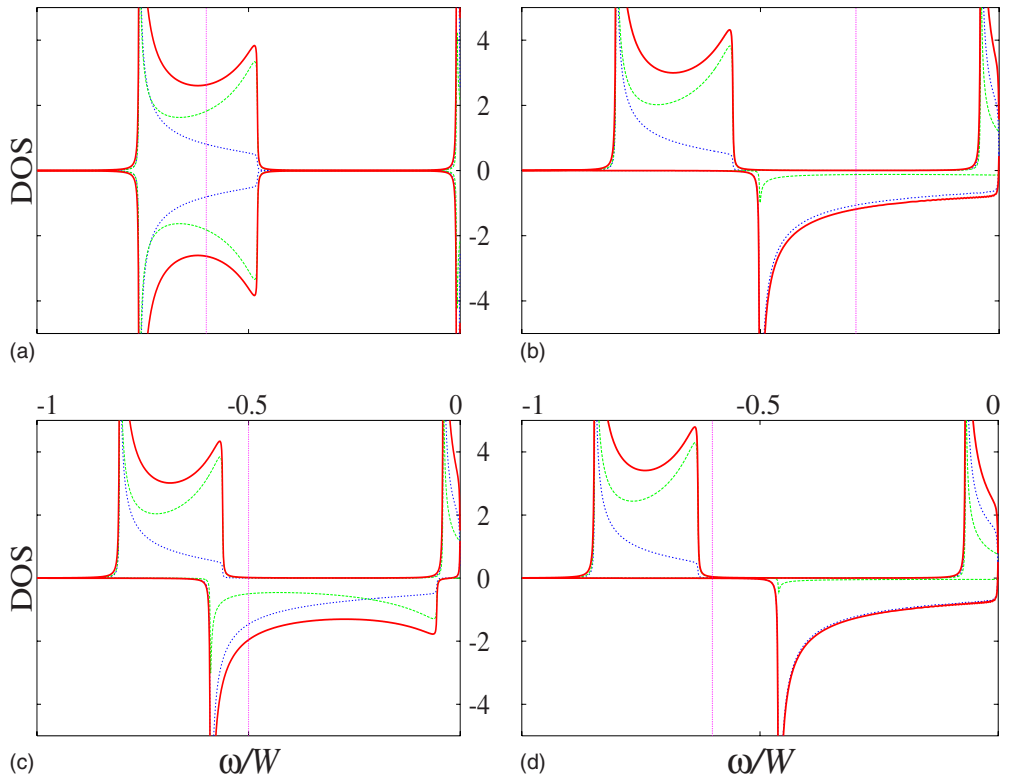

FIG. 3. (Color online) DOS in units of W for the same parameters as in Fig. 1 and $\mu/W=-0.6$, $I/W=0.5$ (top left), corresponding to a PM metallic phase; $\mu/W=-0.3$, $I/W=2.0$ (top right), corresponding to a fm half-metallic phase; $\mu/W=-0.5$, $I/W=1.0$ (bottom left), corresponding to a FM half-metallic phase; and $\mu/W=-0.6$, $I/W=3.0$ (bottom right), corresponding to a FFM insulating phase. The values of the DOS for majority and minority spins are plotted with positive and negative signs, respectively. The solid curves represent the full DOS. The s and d contributions are represented by the thin lines. The s contribution is weaker in the lowest band and stronger in the other bands.

line SC host. The Hamiltonian $\mathcal{H}$ of the Bloch states of the SC, which are annihilated (created) by the operator $s^{(+)}$, is written as

$$\mathcal{H} = \mathcal{H}_0 + \mathcal{V}(+\boldsymbol{\rho}/2) + \mathcal{V}(-\boldsymbol{\rho}/2), \tag{14}$$

where

$$\mathcal{H}_0 = \sum_{\mathbf{K},\sigma} \varepsilon(\mathbf{K}) s^+_{\mathbf{K},\sigma} s_{\mathbf{K},\sigma}, \tag{15}$$

is the Hamiltonian of a bulk SC in the absence of the FM strings, $\varepsilon(\mathbf{K})$ is the corresponding quasiparticle spectrum, and

$$\mathcal{V}(\pm\boldsymbol{\rho}/2) = -\sum_{\mathbf{K},\mathbf{K}'} \sum_{\sigma,\sigma'} s^+_{\mathbf{K},\sigma} \{U_{\mathbf{K},\mathbf{K}'}(\pm\boldsymbol{\rho}/2)\delta_{\sigma,\sigma'} + J_{\mathbf{K},\mathbf{K}'}(\pm\boldsymbol{\rho}/2) \times [\boldsymbol{\sigma}\cdot\mathbf{M}(\pm\boldsymbol{\rho}/2)]_{\sigma,\sigma'}\} \times s_{\mathbf{K}',\sigma'} \exp[\pm i(\mathbf{k} - \mathbf{k}')\cdot\boldsymbol{\rho}/2] \tag{16}$$

describes the interaction of the SC host with two parallel FM strings directed along the z axis and intersecting the plane perpendicular to the z axis at the points $\mathbf{r}=\pm\boldsymbol{\rho}/2$. We use here the same notation for position vectors and wave vectors, adopted in Sec. II.

As we discussed in Sec. II, we treat the spin density of the strings as classical. Therefore, the vector $\mathbf{M}(\pm\boldsymbol{\rho}/2)$ represents the mean magnetization of the "right" $(+\boldsymbol{\rho}/2)$ and "left" $(-\boldsymbol{\rho}/2)$ strings. We assume the vectors $\mathbf{M}(\pm\boldsymbol{\rho}/2)$ to be directed either parallel or antiparallel to the z axis: $\mathbf{M}(\pm\boldsymbol{\rho}/2)=M\mathbf{n}_\pm$, where $\mathbf{n}_\pm$ are unit vectors. For the sake of simplicity, we also assume the interaction $\mathcal{V}(\pm\boldsymbol{\rho}/2)$ to be homogeneous in the z direction and local in the perpendicular plane, so that $U_{\mathbf{K},\mathbf{K}'}(\pm\boldsymbol{\rho}/2)=U\delta_{\kappa,\kappa'}$ and $J_{\mathbf{K},\mathbf{K}'}(\pm\boldsymbol{\rho}/2)=J\delta_{\kappa,\kappa'}$.

Let us analyze the system within a single band approach. The Green's function associated with Hamiltonians (14)–(16) is given by

$$G_{\sigma\sigma'}(\mathbf{K},\mathbf{K}',\omega) = \delta_{\mathbf{K},\mathbf{K}'}\delta_{\sigma,\sigma'}G^0(\mathbf{K},\omega) + \delta_{\kappa,\kappa'}G^0(\mathbf{K},\omega)T_{\sigma\sigma'}(\mathbf{K},\mathbf{K}',\omega)G^0(\mathbf{K}',\omega), \tag{17}$$

where $G^0(\mathbf{K},\omega)=[\omega-\varepsilon(\mathbf{K})]^{-1}$ is the Green's function of the bulk SC, and the additional term appears due to the interaction $\mathcal{V}(\pm\boldsymbol{\rho}/2)$ with the strings, whose expression is found in Eq. (16). Here $T_{\sigma\sigma'}(\mathbf{K},\mathbf{K}',\omega)=Q_{\sigma\sigma'}(\mathbf{K},\mathbf{K}',\omega)/\Delta(\kappa,\omega)$ is full t matrix of the multiple scattering of carriers by two parallel strings inserted in the SC host. The explicit expression for the numerator Q is lengthy and will be omitted since it plays no role in the forthcoming discussion. The determi-

nant in the denominator of the t matrix may be written as

$$\Delta = D^2 - 2g^2(K^2 + J^2M^2C) + g^4(U^2 - J^2M^2)^2, \quad (18)$$

where

$$D = 1 - (U+K)g_0 = (1 - Ug_0)^2 - J^2M^2g_0^2, \quad (19)$$

$$g_0 = g_0(\kappa,\omega) \equiv \sum_{\mathbf{k}} G^0(\mathbf{K},\omega), \quad (20)$$

and

$$g = g(\kappa,\omega) \equiv \sum_{\mathbf{k}} G^0(\mathbf{K},\omega)\exp(i\mathbf{k}\cdot\boldsymbol{\rho}). \quad (21)$$

The poles of the t matrix give the single-particle spectrum of the system. It should be noted that the determinant Δ [Eq. (18)] depends parametrically on both the mutual orientation of the magnetic moments of the strings $[C=(\mathbf{n}_+\cdot\mathbf{n}_-)]$ and on the distance between them $(\rho\equiv|\boldsymbol{\rho}|)$. Since we consider the case when the Fermi level is located inside the SC band gap, only the solutions of the equation $\Delta(\omega)=0$ with negative energies $(\omega<0)$ will be discussed below.

If the interstring distance tends to infinity, $\rho\to\infty$ (accordingly, $g\to 0$), the isolated string limit is recovered. As we discussed in Sec. II, in the system with a short-range attractive potential of a linear defect, there is a localized state for a particle moving perpendicular to the defect axis. If the defect is magnetic, the twofold spin degeneracy of this state is removed due to the exchange interaction. In the case of the single string with $U<0$ and $JM\neq 0$, the spectrum is simply given by the equation $D(\omega)=0$, i.e., $g_0^{-1}(\kappa,\omega)=U\pm JM$. In what follows, for the sake of definiteness, we assume that $|U|>|JM|$, as it is commonly the case.

In the case of the two-string defect, the localized states of the single-string defect are split into bonding and antibonding combinations. The splitting is proportional to the overlap integral of wave functions localized at different strings, i.e., to the value of $(g/g_0)^2$. As a consequence of quantization of the transverse (relative to the string axis) propagation of carriers, four one-dimensional subbands are formed inside the SC gap: $\omega=\omega_i(\kappa)$, $i=1,2,3,4$, where i is the subband index.

For the sake of simplicity, we express the electron spectrum in the form $\varepsilon(\mathbf{K})=\varepsilon_\perp(\mathbf{k})+\varepsilon_\parallel(\kappa)$ and in the following replace the transverse index $\perp$ by the subband index, i.e., assign $\varepsilon_\perp=\varepsilon_i$. Taking into account Eq. (17), one can write the variation in DOS caused by the two-strings defect as

$$\delta\mathcal{N}(\omega) = \sum_i \int d\varepsilon_\parallel \mathcal{N}_1(\varepsilon_\parallel)\delta[\omega - \omega_i(\kappa)], \quad (22)$$

where $\omega_i(\kappa)=\varepsilon_i+\varepsilon_\parallel(\kappa)$ is ith branch of the electron spectrum, which has been defined above as a solution of the equation $\Delta(\omega)=0$; the one-dimensional DOS is introduced in convenient way to promote wave vector sums to energy integral, $N_\parallel^{-1}\Sigma_\kappa\to\int a d\kappa/(2\pi)\to\int d\varepsilon_\parallel\mathcal{N}_1(\varepsilon_\parallel)$, where a is a crystal lattice spacing of the SC. The value ε_i determines the minimum of the ith subband with respect to edge of three-dimensional band of the SC host.

In order to carry out concrete calculations, we adopt for the band electron energy the parabolic form $\varepsilon(\mathbf{K})=(\mathbf{k}^2+\kappa^2)/(2m^*)$, where $m_\parallel^*=m_\perp^*=m^*$ is effective mass near bottom of the band. On the one hand, the effective-mass approach is quite suited because actual quasiparticle energies are small as compared to the width of the conduction band, W: $|\omega|\ll W$. On the other hand, this assumption allows to simplify the calculations and obtain analytical results. Indeed, the functions g_0 [Eq. (20)] and g [Eq. (21)] take the fairly simple forms

$$g_0 = -\mathcal{N}_2\ln(1+E^{-1}), \quad g = -2\mathcal{N}_2K_0(R\sqrt{E}), \quad (23)$$

where the dimensionless units are used: $E=|\varepsilon|/\varepsilon_0$, $R=\rho\sqrt{2m^*\varepsilon_0}$; $\varepsilon=\omega-\varepsilon_\parallel$, ε_0 $(\varepsilon_0\ll W)$ is the cutoff energy which can be related to the column radius $r_0\approx(2m^*\varepsilon_0)^{-1/2}$, $\mathcal{N}_2=m^*a^2/(2\pi)$, and $K_0(\eta)$ is the modified Bessel function of the second kind.

Inserting g_0 and g [Eq. (23)] into expression (18), one may present the equation $\Delta(\omega)=0$ in the form

$$(Y-1)^4 - 2(A+B)(Y-1)^2 - 4AB(Y-1) - 2ABCY + (A+B-AB)^2 - 2AB = 0, \quad (24)$$

where $Y^{-1}=u\ln(1+E^{-1})$, $A=A(\omega)=(g/g_0)^2$, $B=(JM/U)^2$, and $u=\mathcal{N}_2|U|$. We notice several specific features of the solutions of Eq. (24), which are discrete levels energies $(\varepsilon=\varepsilon_i)$. If $C\neq -1$, Eq. (24) has four real roots E_i (we label the solutions such that $E_1>E_2>E_3>E_4$) at sufficiently large distance $R>R_4$, three roots $(E_1>E_2>E_3)$ in an interval $R_3<R<R_4$, and two roots $(E_1>E_2)$ in a region $R<R_3$. This means that there are some characteristic interstring distances for which a state leaves the band gap and enters the continuum. At some intermediate point belonging to the interval (R_3,R_4), the terms E_2 and E_3 intersect each other. When the distance R becomes very large, the energy E tends to the value $E_0^{(\pm)}$ of the localized electron state in the case of a single-string defect in the host. We denote the solutions of Eq. (24) for the case of the parallel (FM) configuration of magnetic moments of the strings $(C=1)$ by $E_{1,2,3,4}^{(f)}$.

For the antiparallel (i.e., AFM) configuration of magnetic moments of the strings $(C=-1)$ when the total magnetization of the system is equal to zero, the spin splitting of the localized states disappears and a pair of twofold-degenerate subbands is left $\omega_i^{(a)}(\kappa)=\varepsilon_i^{(a)}+\varepsilon_\parallel(\kappa)$, $i=1,2$. We denote the corresponding solutions of Eq. (24) as $E_{1,2}^{(a)}$. The solution $E_2^{(a)}$ exists under the condition $R>2/(1-B)$, and is such that $E_1^{(a)}>E_2^{(a)}$ for all R and B.

The solutions of Eq. (24) can be obtained numerically. In Fig. 4 we plot a typical variation in the level positions ε_i as a function of the interstring distance ρ (E vs R) at given dimensionless interaction constant u and mutual orientation of the moments $C=\pm 1$. It is important to notice that $E_1^{(f)}>E_1^{(a)}>E_2^{(f)}>E_3^{(f)}>E_2^{(a)}>E_4^{(f)}$, as it can be seen in Fig. 4.

In the model under consideration, the DOS inside the bulk band gap [Eq. (22)] has a form

$$\delta\mathcal{N}(\omega) = \sum_i \frac{a\sqrt{2m^*}}{2\pi\sqrt{\omega-\varepsilon_i}}h(\omega-\varepsilon_i), \quad (25)$$

where the sum is carried over the states with $\varepsilon_i<0$, and h is the Heaviside function.

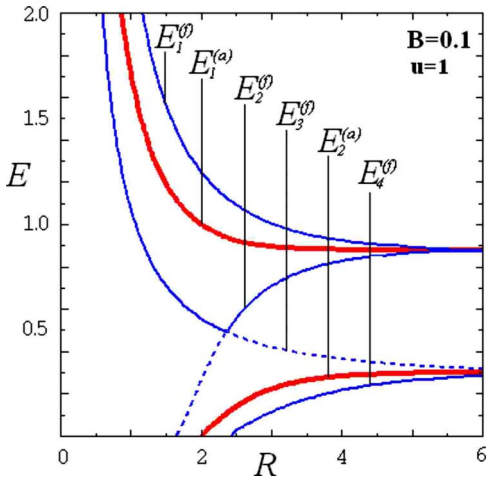

FIG. 4. (Color online) The variation in the subband edge position $E_i^{(f)}(R)$ and $E_i^{(a)}(R)$ with the interstring distance R at $B=0.1$ and $u=1$. The energy state $E_3^{(f)}(R)$ is depicted by the dashed line.

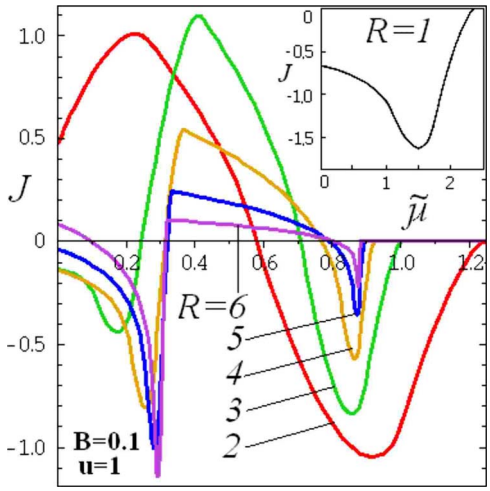

FIG. 5. (Color online) The calibrated exchange integral dependence on the Fermi-level position $J(\tilde{\mu})$ at different values of the interstring distance R. In the inset is $J(\tilde{\mu})$ at $R=1$.

The one-dimensional states split off the band continuum of the bulk SC are partly filled with quasiparticles having been transferred from Mn atoms inside the columns and/or from Mn atoms in the host. Strictly speaking, it would be necessary to study the system for different mutual orientations of the magnetic moments $\mathbf{M}(\pm\boldsymbol{\rho}/2)$, at fixed total number of electrons in the system, consisting of the SC host and of the embedded FM strings. However, this procedure is too complex. Therefore we restrict our analysis to collinear magnetic configurations, FM and AFM, and focus only on the situation when the Fermi level μ is fixed below the band edge of the nondegenerate SC host. In this case, the physical properties can be described in terms of the excess grand-canonical thermodynamic potential,

$$\delta\Omega = \int_{-\infty}^{\mu} (\omega - \mu)\,\delta\mathcal{N}(\omega)d\omega, \tag{26}$$

where $\delta\mathcal{N}(\omega)$ is read off Eq. (25). The exchange integral is calculated as

$$I_c = \delta\Omega^{(f)} - \delta\Omega^{(a)}, \tag{27}$$

where $\delta\Omega^{(f)}$ and $\delta\Omega^{(a)}$ are the specific expressions of $\delta\Omega$ [Eq. (26)] for FM and AFM alignments of the moments $\mathbf{M}(\pm\boldsymbol{\rho}/2)$, respectively. After integration, one obtains the exchange integral as a function of μ,

$$I(\mu) = I_0\left[2\sum_i (E_i^{(a)} - \tilde{\mu})^{3/2} - \sum_i (E_i^{(f)} - \tilde{\mu})^{3/2}\right], \tag{28}$$

where the sum is carried over the occupied states, $E_i^{(f,a)} > \tilde{\mu}$, $\tilde{\mu} = |\mu|/\varepsilon_0$, and $I_0 = 2a\sqrt{2m^*\varepsilon_0^3}/(3\pi)$. A set of curves $I(\mu)$ [Eq. (28)] is represented in Fig. 5, where the dimensionless quantity $J(\tilde{\mu}) = I(\mu)\exp(R)/I_0$, which includes the scaling prefactor $\exp(R)$, is plotted for different values of R.

The most important result concerns the magnitude and character of the coupling, which strongly depend on the filling of confinement-induced states ω_i and on the interstring distance. Figure 5 shows that the exchange interaction at short distance ($R \lesssim 1$) is FM, whereas, with increasing interstring distance (at given B and u), the exchange integral $I(\mu)$ as a function of μ can change its sign up to three times. Thus, varying the Fermi level or the interstring distance one could switch the exchange coupling between FM and AFM.

The asymptotic behavior of the exchange integral at large interstring distance is given by the expression $I_c(\rho) \sim \exp(-\rho/\rho_0^{(\pm)})$, where the characteristic length

$$\rho_0^{(\pm)} = \left[\frac{2m^* a}{\sqrt{\pi}}\sqrt{\varepsilon_0(|U| \pm |JM|)}\right]^{-1} \tag{29}$$

is the scale of the coupling decay in dimensional units. Unfortunately, at present, the insufficiency of experimental data does not allow for an accurate estimate of the physical values of the various parameters. We can only give a rough estimate of the characteristic length $\rho_0^{(\pm)} \approx 1.5$–$1.8$ nm, which is based on the following parameters: $m = 0.04m_0$, $a = 0.56$ nm, $r_0 \approx 1$ nm, and $|U| \pm |JM| \approx 3$–4 eV.

IV. CONCLUSION

In summary, to qualitatively analyze the magnetic properties of the phase-separated (Ge,Si):Mn alloys with self-organized nanocolumns,[12–15] we proposed a model which accounts for the onset of a spin-polarized state within an isolated nanocolumn, described as an ideal FM string embedded into the SC host. We then considered an effective semiphenomenological Hamiltonian to describe the coupling between the FM string and the SC host and discussed the mechanism for the exchange coupling between two parallel strings. We demonstrated that in the case of a nondegenerate SC host, when the Fermi level is located inside the energy gap, the quasiparticle transitions between the confinement-induced spin-polarized one-dimensional states and the three-dimensional states of the SC host lead to an efficient interstring coupling. This could be designated as a "carrier-confinement-mediated" mechanism of the indirect magnetic coupling. The related exchange integral can switch its sign between FM and AFM as the interstring distance or the fill-

ing of quasi-one-dimensional spin-polarized subbands varies. The coupling magnitude decays exponentially with the interstring distance. We point out that we neglected the presence of an impurity band in the system. Experimentally, the situation is far from settled. An insulating behavior of the resistivity as a function of temperature has been reported for Ge:Mn DMS,[3] compatible with an Efros-Shklovski variable-range hopping conduction mechanism. This behavior would imply that the Fermi level is located below the mobility edge of the Mn-induced impurity band. On the other hand, the variable-range hopping mechanism was questioned, and a behavior of the resistivity consistent with a percolation mechanism associated with bound magnetic polarons with localized holes was proposed.[16] Since we have no experimental evidence for the existence of an impurity band in Ge:Mn DMS with columnar structure, we left the investigation of the transport properties to a later research, when the experimental situation will be clearer, and limited our analysis to the exchange mechanism between the Mn-rich columns. We note, on passing, that an impurity band would enhance the global tendency to ferromagnetism in Ge:Mn DMS,[3] whereas our mechanism accounts for both AFM and FM orders in these systems. In our opinion, the carrier-confinement-mediated mechanism of exchange coupling discussed in this paper may account for the magnetic behavior in the phase-separated (Ge,Si):Mn alloys, although some open problems remain to be solved.

First, we did not address the origin of the columnar structure of Ge:Mn DMS, and rather assumed its existence as a starting phenomenological point. In future, it would be interesting to extend our approach and take into account some of the features considered in Ref. 17, where the problem of the spinodal decomposition and phase separation in GaMnAs DMS has been treated at the first-principles level.

Second, the main assumptions of our model and the results obtained here need to be confirmed by more rigorous *ab initio* calculations; in particular, the quasi-one-dimensional FM character of the spectrum of (Ge,Si):Mn alloys with self-organized nanocolumns has to be established. So far, unfortunately, these calculations have not been performed.

Third, magnetic and transport properties of (Ge,Si):Mn alloys with self-organized nanocolumns are highly sensitive to the effect of magnetic impurities existing into the SC matrix; this effect was neglected in our analysis. As it was mentioned in Sec. I, an AFM coupling between the neighboring nanocolumns and a giant positive MR was observed in the unannealed Ge:Mn films.[15] The acceptors (Mn atoms replacing Ge) and donors (interstitial Mn atoms) in these materials almost completely compensate for each other, while the Fermi level is located lower than the mobility threshold. Due to the annealing, the Mn atoms are redistributed in the bulk and between the matrix and the nanocolumns, as a result of which the fraction of uncompensated acceptors increases, the FM coupling arises between the nanocolumns, and a small negative MR appears. The carrier-confinement-mediated mechanism allows the alternation of the sign of the exchange coupling between nanocolumns to be associated with the change in the position of the Fermi level even in the case of a nondegenerate SC matrix since the sign of the exchange coupling can vary with the filling of spin-polarized states. On the other hand, if the Fermi level after annealing lies above the mobility threshold and the metal-insulator transition occurs, a FM coupling between nanocolumns is accounted for by the standard exchange mechanism of the Ruderman-Kittel-Kasuya-Yoshida (RKKY) type. We point out that a RKKY exchange mechanism mediated by low-density carriers strongly depends on the degree of compensation in the SC host and disappears in nondegenerate DMS with almost complete compensation. On the other hand, our mechanism is almost independent of the carrier concentration in the host.

A final comment concerns the transport anisotropy in DMS with columnar topology. In ideal structures, our model predicts a metallic behavior along the columns, and an insulating (possibly tunneling) behavior in the directions perpendicular to the columns. However, in real systems, compositional and structural fluctuations of the columnar structure would lead to carrier localization inside the quasi-one-dimensional columns, resulting in an overall insulating behavior.

ACKNOWLEDGMENTS

The work was partially supported by the University of the Basque Country (Grant No. 9/UPV 00206.215-13639/2001), by Spanish Ministerio de Ciencia y Tecnología (Grant No. FIS 2004-06490-C03-01), and by RFBR (Grant No. 07-02-00114-a).

[1] Y. D. Park, A. Y. Hanbicki, S. Erwin, C. Hellberg, J. Sullivan, J. Mattson, T. F. Ambrose, A. Wilson, G. Spanos, and B. Jonker, Science **295**, 651 (2002).

[2] S. Cho, S. Choi, S. C. Hong, Y. Kim, J. B. Ketterson, B.-J. Kim, Y. C. Kim, and J.-H. Jung, Phys. Rev. B **66**, 033303 (2002).

[3] A. P. Li, J. F. Wendelken, J. Shen, L. C. Feldman, J. R. Thompson, and H. H. Weitering, Phys. Rev. B **72**, 195205 (2005).

[4] R. R. Gareev, Yu. V. Bugoslavsky, R. Schreiber, A. Paul, M. Sperl, and M. Döppe, Appl. Phys. Lett. **88**, 222508 (2006).

[5] S. Ahlers, D. Bougeard, N. Sircar, G. Abstreiter, A. Trampert, M. Opel, and R. Gross, Phys. Rev. B **74**, 214411 (2006).

[6] E. Biegger, L. Staheli, M. Fonin, U. Rudiger, and Yu. S. Dedkov, J. Appl. Phys. **101**, 103912 (2007).

[7] P. De Padova, J. P. Ayoub, I. Berbezier, P. Perfetti, C. Quaresima, A. M. Testa, D. Fiorani, B. Olivieri, J.-M. Mariot, A. Taleb-Ibrahimi, M. C. Richter, O. Heckmann, and K. Hricovini, Phys. Rev. B **77**, 045203 (2008).

[8] M. Bolduc, C. Awo-Affouda, A. Stollenwerk, M. B. Huang, F. G. Ramos, G. Agnello, and V. P. LaBella, Phys. Rev. B **71**, 033302 (2005).

[9] A. Wolska, K. Lawniczak-Jablonska, M. Klepka, M. S. Walczak, and A. Misiuk, Phys. Rev. B **75**, 113201 (2007).

[10] S. Zhou, K. Potzger, G. Zhang, A. Mucklich, F. Eichhorn, N. Schell, R. Grotzschel, B. Schmidt, W. Skorupa, M. Helm, J. Fassbender, and D. Geiger, Phys. Rev. B **75**, 085203 (2007).

[11] L. Zeng, E. Helgren, M. Rahimi, F. Hellman, R. Islam, B. J. Wilkens, R. J. Culbertson, and D. J. Smith, Phys. Rev. B **77**, 073306 (2008).

[12] Y. Zhang, Q. Jiang, D. Smith, and J. Ducker, J. Appl. Phys. **98**, 033512 (2005).

[13] M. Jamet, A. Barski, T. Devillers, V. Poydenot, R. Dujardin, P. Bayle-Guillemaud, J. Rothman, E. Bellet-Amalric, A. Marty, J. Cibert, R. Mattana, and S. Tatarenko, Nature Mater. **5**, 653 (2006).

[14] T. Devillers, M. Jamet, A. Barski, V. Poydenot, P. Bayle-Guillemaud, E. Bellet-Amalric, S. Cherifi, and J. Cibert, Phys. Rev. B **76**, 205306 (2007).

[15] A. P. Li, C. Zeng, K. van Benthem, M. F. Chisholm, J. Shen, S. V. S. Nageswara Rao, S. K. Dixit, L. C. Feldman, A. G. Petukhov, M. Foygel, and H. H. Weitering, Phys. Rev. B **75**, 201201(R) (2007).

[16] N. Pinto, L. Morresi, M. Ficcadenti, R. Murri, F. D'Orazio, F. Lucari, L. Boarino, and G. Amato, Phys. Rev. B **72**, 165203 (2005).

[17] K. Sato, H. Katayama-Yoshida, and P. H. Dederichs, Jpn. J. Appl. Phys., Part 2 **44**, L948 (2005).